Supplementary Material

S1. Details about the MGB hydrological–hydrodynamic model

In this section, a brief overview of the MGB structure used for hydrological modeling in South America is presented. Basically, this is a vector-based model that uses conceptual equations to simulate the terrestrial hydrological cycle, including soil water and energy budget, evapotranspiration, canopy interception, surface, subsurface and groundwater runoff, as well as flow routing along river channels (**Figure S1.1**). The following sections are described according to the initial model development by Collischonn et al., (2007) and further improvements by Paiva et al., (2011), Pontes et al., (2017) and Fleischmann et al., (2018).
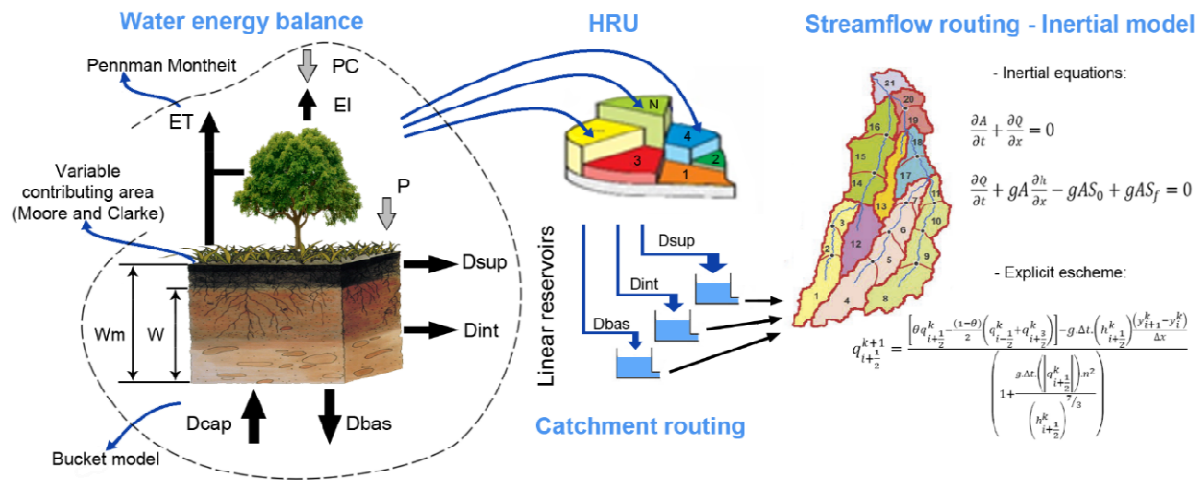
Figure S1.1. Schematic representation of MGB model general structure.

S1.1 Water and energy balance

In the model, the basin is discretized into unit-catchments, which are further divided in hydrological response units (HRU) (Beven, 2001) that are usually produced by the combination of soil and land cover maps. Vertical water and energy budgets are computed independently for each HRU of each unit-catchment. Soil water balance is computed considering a single soil layer (bucket model), according to:

$$W_{i,j}^t = W_{i,j}^{t-1} + \left(P_i - ET_{i,j} - Dsup_{i,j} - Dint_{i,j} - Dbas_{i,j} + Dinf_{i,j}\right)\Delta t$$

<div align="right">Eq. S1.1.1</div>

Where: t, i and j, are indexes related to time step, unit-catchment and HRU, respectively; Wm is the water storage capacity in the soil layer [mm]; P is the precipitation that reaches the soil [mm Δt^{-1}]; ET is the evapotranspiration from soil [mm Δt^{-1}]; $Dsup$ is the surface runoff [mm Δt^{-1}]; $Dint$ is the subsurface flow [mm Δt^{-1}]; $Dbas$ is the flow to the groundwater reservoir [mm Δt^{-1}]; $Dinf$ is the infiltration of flooded areas to the soil [mm Δt^{-1}] and; Δt is the time step for water budget, usually equal to 1 day.

Soil infiltration and runoff are computed based on the variable contributing area concept of the ARNO model (Todini, 1996):

$$Dsup_{i,j} = \Delta t P_i - \left(Wm_j - W_{i,j}^{t-1} \right), for\ y \leq 0$$

Eq. S1.1.2

$$Dsup_{i,j} = \Delta t P_i - (Wm_j - W_{i,j}^{t-1}) + Wm_j \left[\left(1 - \frac{W_{i,j}^{t-1}}{Wm_j} \right)^{\frac{1}{b_j+1}} - \frac{\Delta t P_i}{Wm_j (b_j + 1)} \right]^{b_j+1}, \quad for\ y > 0$$

Eq. S1.1.3

$$y = \left[\left(1 - \frac{W_{i,j}^{t-1}}{Wm_j} \right)^{\frac{1}{b_j+1}} - \frac{\Delta t P_i}{Wm_j (b_j + 1)} \right]$$

Eq. S1.1.4

Where W is the current soil water storage [mm]; Wm is the maximum water storage capacity [mm]; b is a parameter that controls the distribution of water storage capacity of the soil [-]; P is the precipitation that reaches the soil [mm];

Subsurface flow is obtained using a function similar to the Brooks and Corey unsaturated hydraulic conductivity equation (Rawls et al., 1993):

$$Dint_{i,j} = Kint_j \left(\frac{W_{i,j} - Wz_j}{Wm_j - Wz_j} \right)^{\left(3 + \frac{2}{\lambda_j}\right)}$$

Eq. S1.1.5

Where $Kint$ is the saturated hydraulic conductivity [mm Δt^{-1}], λ is the soil porosity index [-] and Wz is the lower limit below which there is no subsurface flow ($W_Z = 0.1Wm$).

Percolation from soil layer to groundwater is calculated according to a simple linear relation between soil water storage and maximum soil water storage:

$$Dbas_{i,j} = Kbas_j \left(\frac{W_{i,j} - Wc_j}{Wm_j - Wc_j} \right)$$

Eq. S1.1.6

Where *Kbas* is a parameter that gives the percolation rate to groundwater in the case of saturated soil [mm Δt^{-1}].

Infiltration from floodplain into soil column is computed as a two–way coupled scheme between hydrological vertical balance and hydrodynamic module (see next section, **Eq. S1.2.9**). It is assumed that infiltration rate is linearly dependent on the degree of soil saturation, thus reaching its maximum when soil is completely dry (Fleischmann et al., 2018).

$$D^t_{inf_i} = \frac{A^t_{fl_i}}{A_i} \cdot K_{inf} \left(1 - \frac{W^t_i}{Wm} \right)$$

Eq. S1.1.7

Where Afl_i is the flooded area at unit-catchment i [km²], *A* is the unit-catchment area [km²], K_{inf} the infiltration rate that occurs when the whole unit-catchment is flooded and soil is totally dry [mm Δt^{-1}], *w* is the soil water content and *Wm* is the maximum soil water storage.

Runoff generated (*Dsup*, *Dint* and *Dbas*) within unit-catchments is routed to the drainage network using three independent linear reservoirs (**Eqs. S1.1.8–S1.1.10**). For surface and subsurface reservoirs, streamflow releases (*Q*) are controlled by the time of concentration computed with Kirpich formula similarly to Ludwig and Bremicker (2006).

$$Q_{sup_i} = \frac{V_{sup_i}}{Cs \left[3600 \left(0.868 \frac{L_i}{\Delta H_i} \right)^{0.385} \right]}$$

Eq. S1.1.8

$$Q_{int_i} = \frac{V_{int_i}}{Ci \left[3600 \left(0.868 \frac{L_i}{\Delta H_i} \right)^{0.385} \right]}$$

Eq. S1.1.9

$$Q_{bas_i} = \frac{V_{bas_i}}{Cb}$$

Eq. S1.1.10

Where *Vsup*, *Vint* and *Vbas* are the surface, subsurface and groundwater reservoir volumes, respectively [m³]; L_i and ΔH_i are, respectively, the length and the elevation difference of the largest flowpath between unit-catchment border and the main river [m]; *Cs*

and Ci are parameters that correct the prior estimate of time of concentration (given by Kirpich formula) [-]; Cb is the groundwater residence time, which can be estimated from hydrograph recession considering a long dry period [s].

Precipitation is assumed to be stored in canopy until maximum interception storage capacity is reached, which is determined for each HRU based on the vegetation leaf area index. Energy budget and evaporation from soil, vegetation and canopy to the atmosphere is estimated by the Penman–Monteith equation (Shuttleworth, 1993), using an approach similar to Wigmosta et al., (1994):

$$E = \left[\frac{\Delta \left(R_L - G \right) + \rho_a c_p \frac{e_s - e_d}{r_a}}{\Delta + \gamma \left(1 + \frac{r_s}{r_a} \right)} \right] \frac{1}{\lambda \rho_w}$$

Eq. S1.1.11

Where E is the potential evaporation rate [m s^{-1}]; R_L is the net radiation [MJ m^{-2} s^{-1}]; G is the soil heat flux [MJ m^{-2} s^{-1}]; λ is the latent heat of vaporization [MJ kg^{-1}]; Δ is the gradient of the saturated vapour pressure–temperature function [kPa ºC^{-1}]; A is the available energy [MJ m^{-2} s^{-1}]; ρa is the air density [kg m^{-3}]; ρ_w is the specific mass of water [kg m^{-3}]; c_p is the specific heat of moist air [MJ kg^{-1} ºC^{-1}]; ($e_s - e_d$) represents the vapor pressure deficit [kPa]; γ is the psychrometric constant [kPa ºC^{-1}]; r_s is the surface resistance of the land cover [s m^{-1}] and r_a is the aerodynamic resistance [s m^{-1}].

Firstly, intercepted water is evaporated (*EI*) at the potential rate E. The evapotranspiration (*ET*) of the vegetated soil (soil evaporation + plant transpiration) is calculated using **Eq. S1.1.11**, weighted by the remaining evaporative demand ([*E–EI*]/*E*) in order to respect the overall energy balance. In addition, *ET* is reduced in situations of water stress, and it is assumed that soil conditions restrict evapotranspiration if current soil water storage is below a threshold value given by $W_L = Wm / 2$. In the range between this limit and the wilting point, surface resistance increases according to:

$$r_s = r_{s_{j,m}} \left(\frac{W_L - W_{wp}}{W_{i,j} - W_{wp}} \right)$$

Eq. S1.1.12

Where W_{wp} is the wilting point, equal to 10% of maximum soil capacity (Wm) [mm]; $r_{s_{j,m}}$ is the vegetation-dependent minimum surface resistance, in conditions not affected by soil moisture [s m^{-1}] and m is the month index.

S1.2 Flow routing (local inertial equation)

Flow in natural channels is governed by 1D full Saint–Venant equations (Cunge et al., 1980), expressed by continuity (**Eq. S1.2.1**) and momentum conservation (**Eq. S1.2.2**):

$$\frac{\partial A}{\partial t} + \frac{\partial Q}{\partial x} = q,$$

Eq. S1.2.1

$$\frac{\partial Q}{\partial t} + \frac{\partial}{\partial x}\left(\frac{Q^2}{A}\right) + gA\frac{\partial(h+z)}{\partial x} + \frac{gn^2\,|Q|\,Q}{R_h^{4/3}A} = 0$$

$$\underbrace{}_{\substack{\text{Local}\\\text{Acceleration}}} \quad \underbrace{}_{\substack{\text{Convective}\\\text{Acceleration}}} \quad \underbrace{}_{\substack{\text{Pressure +}\\\text{Bed gradients}}} \quad \underbrace{}_{\text{Friction}}$$

Eq. S1.2.2

Where Q is the river discharge [m³ s^{-1}], q is the lateral inflow [m³ s^{-1}], A is the flow cross-section area [m²], h is the flow depth [m], z is the channel bed elevation, relative to a datum [m]; R_h is the hydraulic radius [m], g is the acceleration due to gravity [m s^{-2}], and n is the Manning coefficient [s m$^{-1/3}$].

In order to deal with a wide range of flow conditions, the MGB solves the momentum equation using the local inertial approximation proposed by Bates et al., (2010). Using a forward in time finite difference scheme and neglecting the convective acceleration term, the momentum equation can be written as:

$$\frac{Q^{t+1} - Q^t}{\Delta t} + gA\frac{\partial(h^t+z)}{\partial x} + \frac{gn^2\,|Q^t|\,Q^t}{R_h^{4/3}A} = 0$$

Eq. S1.2.3

In **Eq. S1.2.3**, flow variables in the friction term ($|Q^t|Q^t$) are written semi-implicitly ($|Q^t|Q^{t+1}$), which in turn can be rearranged into an explicit form of flow calculation:

$$Q^{t+1} = \frac{Q^t - \Delta t\,gA\frac{\partial(h^t+z)}{\partial x}}{\left(1 + \frac{\Delta t\,gn^2|Q^t|}{R_h^{4/3}A}\right)}$$

Eq. S1.2.4

Assuming a rectangular channel and approximating the hydraulic radius with the flow depth (h) for wide, relatively shallow rivers, we can divide **Eq. S1.2.4** by the flow constant width (B) to obtain an equation in terms of flow per unit width:

$$q^{t+1} = \frac{q^t - \Delta t g h^t \frac{\partial\left(h^t + z\right)}{\partial x}}{\left(1 + \frac{\Delta t g h^t n^2 |q^t|}{(h^t)^{10/3}}\right)}$$

Eq. S1.2.5

The resulting local inertial equation (Bates et al., 2010) plays an important role for large-scale simulations in lowland rivers and floodplains areas, and some advantages over a diffusive wave model (which neglects both acceleration terms) include a better physical representation of shallow water flows, as well as the stability improvement for both large depths and small surface water slopes (Yamazaki et al., 2013; de Almeida et al., 2013). Following Almeida et al., (2012) and Neal et al., (2012), the explicit finite difference scheme is applied to a "staggered grid", so that flows at interfaces are used to update water depths at the centers of the numerical grid (i.e., centered in space approximation). Therefore, the momentum equation is written at its final form:

$$q_i^{t+1} = \frac{q_i^t - \Delta t.g\left(B.hflow_i^t\right).Sflow_i^t}{\left(1 + \frac{\Delta t.g.n^2.hflow_i^t.\left|q_i^t\right|}{B.\left(hflow_i^t\right)^{10/3}}\right)}$$

Eq. S1.2.6

Where: Δt is the routing model time step [s]; $q^t{}_{i+1/2}$ and $q^{t+1}{}_{i+1/2}$ are, respectively, the flow from previous and current time step divided by channel width, at the outlet of unit catchment i [m² s^{-1}]; $Sflow_i$ and $hflow_i$ are, respectively, the water surface slope [m m^{-1}] and the effective water depth at the interface between current (i) and downstream ($i+1$) unit-catchment [m].

Note that indexes *i+1/2* are positions of the numerical grid corresponding to the outlets of unit-catchments, which are defined at grid interfaces. Using a similar approach of Neal et al., (2012), *Sflow* and *hflow* are computed as:

$$Sflow_i^t = \frac{(h_{i+1}^t + z_{i+1}) - (h_i^t + z_i)}{\Delta x_i}$$

Eq. S1.2.7

$$hflow_i^t = max\left[h_{i+1}^t + z_{i+1}; h_i^t + z_i\right] - max\left[z_{i+1}; z_i\right]$$

Eq. S1.2.8

Where Δx_i is the flow distance, computed as the average between channel lengths L_i and L_{i+1} ($\Delta x_i \approx L_i \approx L_{i+1}$, according to the fixed-length river discretization, see **sect. S1.3**); h_i and h_{i+1} are the flow depths; z_i and z_{i+1} are the channel bed elevations, respectively, at unit-catchments i and $i+1$.
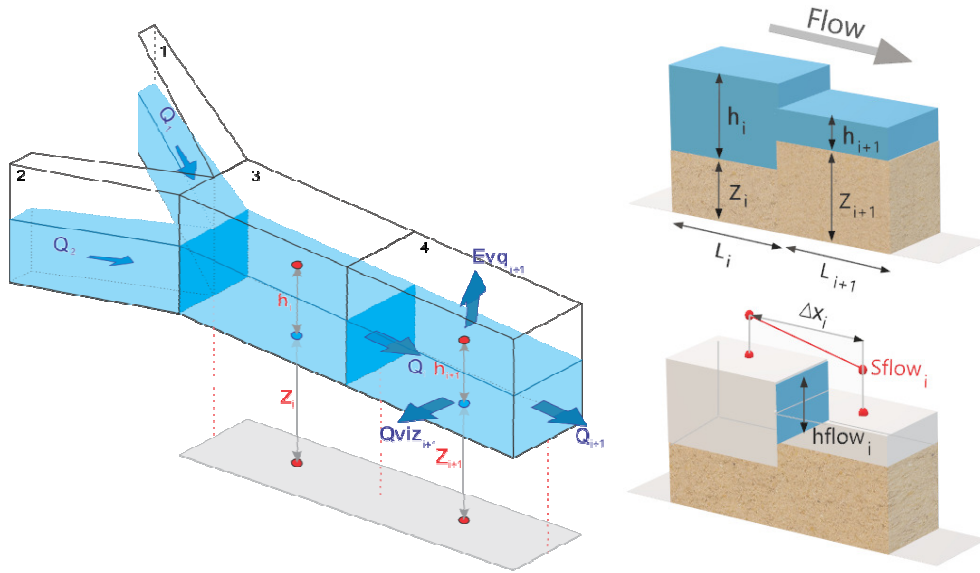
Figure S1.2.1. Schematic representation of MGB flow calculation units.

Discharge is computed after solving **Eq. S1.2.6** and multiplying the q variable by channel width (B), which means that the effective flow area is limited by the rectangular channel geometry. Similar to Yamazaki et al., (2011) and Luo et al., (2017), water mass is instantaneously exchanged between channel and floodplain when bankfull depth is exceeded, whereas water surface elevation of both storages is assumed equal within a given unit-catchment. Total volume (channel + floodplain) is updated using the continuity equation, expressed in terms of:

$$V_i^{t+1} - V_i^t = \left[\sum Q_{in}^t - \sum Q_{out}^t - \left(Evq_i^t - D_{inf_i}^t\right) A_{fl_i}^t / 1000\right] \Delta t$$

Eq. S1.2.9

Where V_i is the total volume stored in channel and floodplains, for unit-catchment i [m^3]; Q_{in} and Q_{out} are, respectively, the inflow and outflow discharge of unit-catchment i [m³ s^{-1}]; Evq_i is the evaporation loss [mm Δt^{-1}] and; $Dinf_i$ is the infiltration from floodplains to soil column [mm Δt^{-1}]. Note in **Figure S1.2.1** that MGB can also route water in multiple directions downstream (Q_{viz}) (Pontes et al., 2017), but this configuration is not used in the current South America version.

Evaporation losses are taken into account by assuming flooded area as open water (i.e., $r_s = 0$) and applying the Penman–Monteith equation (**Eq. S1.1.11**). Therefore, when flooding occurs in a given unit-catchment, the surface area available for soil water budget is reduced proportionally from each HRU, while rainfall over flooded area produces direct surface runoff.

After solving all V^{t+1} in **Eq. S1.2.9**, these values are used to obtain flow depths by interpolating the water volume at each unit-catchment using channel/floodplain profiles (see section **S1.6** for details). Updated flow depths are then used to recompute both *Sflow* and *hflow* variables using **Eqs**. **S1.2.7** and **S1.2.8**, so that flows can be obtained for next time step.

An advantage of the explicit inertial formulation is that model time step is governed by the Courant–Friedrichs–Lewy (CFL) condition. Therefore, the maximum acceptable time step is adaptive and changes according to maximum water depth (**Eq. S1.2.10**):

$$\Delta t = \alpha \frac{\Delta x}{\sqrt{gh_{max}}}$$

Eq. S1.2.10

Where Δx is the flow distance (according to fixed-length discretization); h_{max} is the maximum flow depth in model domain and α is a coefficient that varies between 0.2–0.7 (Bates et al., 2010).

Despite the CFL condition provides the optimum time step needed for flow computation, some issues can arise especially in rivers with higher slopes, which are expected to produce model instabilities. In cases where supercritical flows occur, a flow limiter (**Eq. S1.2.12**) is then invoked to force the Froude number (**Eq. S1.2.11**) below to unity, so that model stability can be further enhanced:

$$F = \frac{v}{\sqrt{gh}} = \frac{Q/A}{\sqrt{gh}} < 1$$

<div align="right">Eq. S1.2.11</div>

$$Q \begin{cases} min\left[Q; B\sqrt{hflow^{1.5}g}\right] & for\ Q \geq 0 \\ max\left[Q; -B\sqrt{hflow^{1.5}g}\right] & for\ Q < 0 \end{cases}$$

<div align="right">Eq. S1.2.12</div>

Where F is the Froude number [-]; v is the mean flow velocity [m s^{-1}]; B is the channel width [m]. Note that the flow limiter also considers reverse flows, which can occur due to backwater effects.

S1.3 Spatial representation of river network in MGB model: definition of unit-catchments by a fixed-length river discretization

As unit-catchments derived from topography (sub-basin approach) are defined between river junctions (Maidment, 2002), the resulting river reaches are characterized by a high variability of lengths that are not suitable for hydrodynamic routing. Therefore, we adopted a fixed-length vector river discretization in order to provide even (and predefined) flow distances between unit-catchments, as well as to facilitate coupling of both hydrological and hydrodynamic modules of MGB. This approach was first mentioned in Pontes et al., (2017) and has been included in the IPH-Hydro Tools GIS package (Siqueira et al., 2016b). Using grids of flow direction, flow accumulation and river networks, the fixed length discretization can be conducted through the following sequence of steps:

S1.3.1. Step 1 – Marking outlets

The first step is to identify all the intermediate outlet points in the stream network. An "intermediate outlet" refers to the very downstream pixel of a given river reach (i.e., between two junctions), as can be seen in the orange boxes presented in **Figure S1.3.1a**. For each pixel in the flow direction grid, if two or more neighboring pixels are drained to the analyzed one, provided that all of them are over the extracted drainage, then a junction is found. Using a 3 × 3 window centered at this point, the grid positions of nearby upstream draining pixels (i.e., intermediate outlets) are stored together with their respective flow accumulated areas. This procedure is repeated until the entire grid is evaluated, and by the end the positions and accumulated area of basin outlet are also stored in conjunction with the intermediate outlets.

S1.3.2. Step 2 – Delineating reaches and unit-catchments by a length threshold

The second step is to segment streams using a specific length as a threshold value, thus providing an even distribution of flow distances. For this, grid positions of the intermediate outlets are initially sorted descending according to their flow accumulated area, so the outlet of the main stream is processed at first. Following the schematic presented in **Figure S1.3.1b**, the procedure then starts at the basin outlet point (green square) using a value of accumulated length equal to 0. Tracing in the upstream direction, the length is accumulated pixel by pixel using Euclidean local distances and the Distance Transforms method (Butt and Maragos, 1998; Paz and Collischonn, 2007), and an identifier value (ID) is assigned to each pixel along the flow path to further distinguish between reaches. Whenever the threshold value of distance is exceeded, as highlighted by the break lines in **Figure S1.3.1b**, the ID is increased by one unit and the accumulated length is reset to zero. This procedure must be constantly repeated, but when a junction is found along the current flowpath, the algorithm selects the upstream pixel with the highest accumulated area (blue squares) to keep tracing until the threshold value of length is met. However, if the length threshold is not achieved when the headwater pixel is found, an extension of the drainage network (dashed line in **Figures S1.3.1b**, **S1.3.1c** and **S1.3.1d**) is created following the pixel with the highest upstream accumulated area. In other words, it results in a "dynamic area threshold" for first order streams, but in this case, length can be lesser than the threshold value once it is topographically limited by headwater catchment boundaries.

After defining all branches in the basin main river, the next intermediate outlet with the highest value of accumulate area is selected (green square) to proceed with the segmentation process, as shown in **Figure S1.3.1c**. However, it is important to mark outlet pixels over the previously segmented flow path as "checked" (white squares). Because the algorithm starts from an intermediate outlet (accumulated length = 0) when tracing in upstream direction, checked pixels must be neglected to avoid redefinition of already processed reaches. Following these constraints, the procedure continues until the entire river network is segmented (**Figure S1.3.2a**).

Finally, all pixels draining to a given reach (i.e., with the same ID) belong to the same unit-catchment, as presented in **Figure S1.3.2b**. The discretization procedure also creates an irregular grid according to topography, despite of the unit-catchment bending at tributaries due to the length threshold constraint.
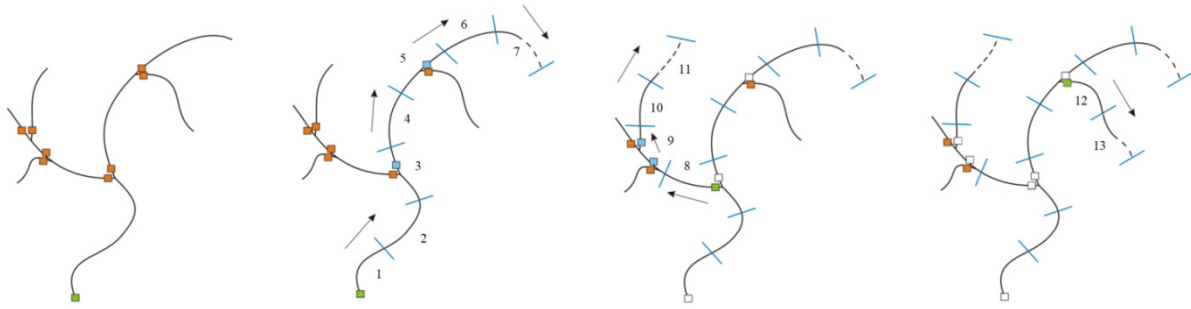
Figure S1.3.1. Procedure of delineating reaches by a length threshold value: (a)Marking intermediate (orange squares) and basin outlet (green square) points, (b)Segmentation starting from basin outlet (green square) and junction overpass following outlet pixels with highest accumulated area (blue squares), (c)Segmentation starting from the next intermediate outlet (green square), ranked in descending order of accumulated area. Intermediate outlet pixels located at previously traced flowpaths (white squares) are ignored if selected for starting a new segmentation.
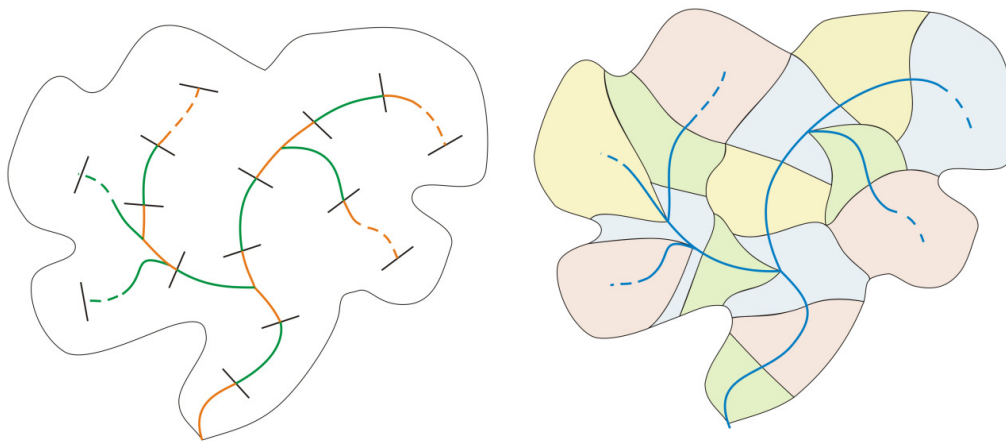
Figure S1.3.2. Schematic representation of the resulting fixed-length vector-based discretization: (a)Final river segmentation: river reaches are separated by break lines and distinguished by colors (orange and green) for visualization purposes; (b)All pixels draining to the same river reach correspond to a given unit-catchment.

Figure S1.3.3 shows an example of the resulting unit-catchments for South America version of MGB, using the above fixed-length discretization approach. Unit-catchments were produced using the flow direction map of HydroSHEDS (Lehner et al., 2008), an upstream area threshold of 1000 km² for river networks and a length threshold of Δx = 15 km. Each unit-catchment centroid represents the location for which precipitation fields are interpolated, as required for the rainfall-runoff module of MGB.
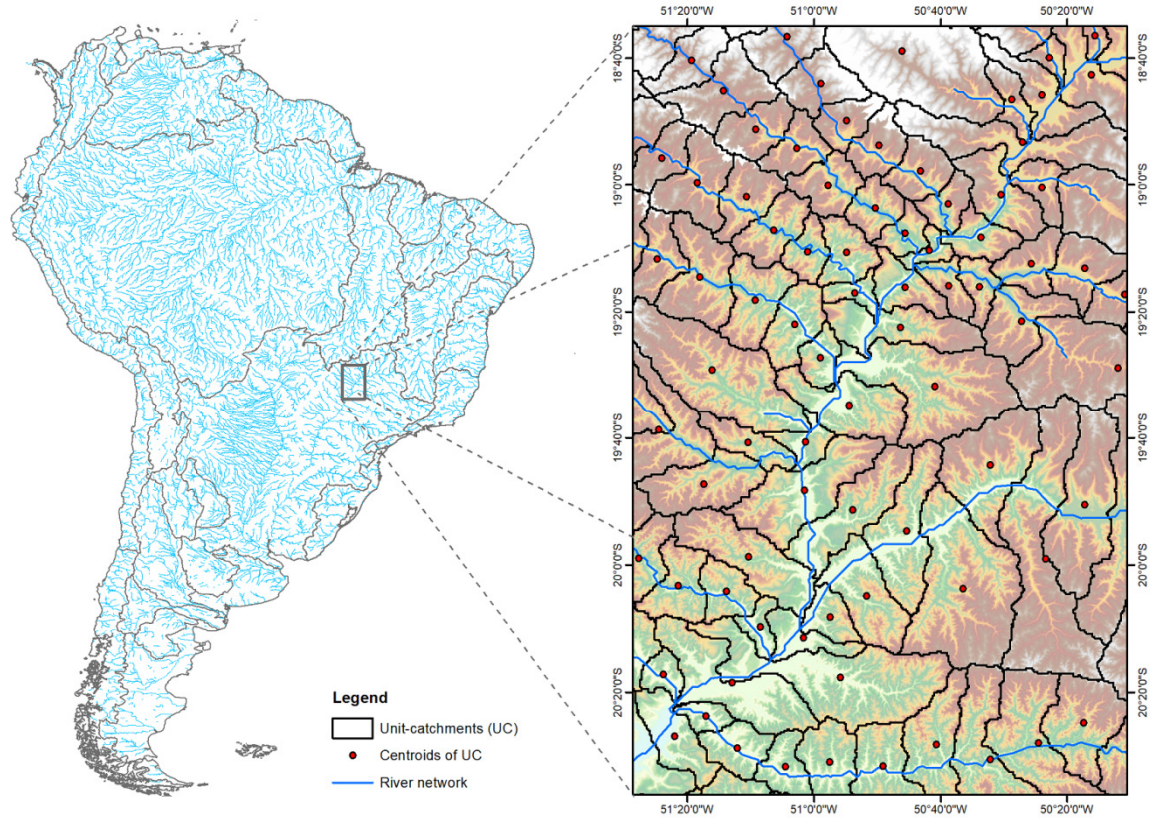
Figure S1.3.3. River drainage networks of South America derived from HydroSHEDS flow direction map (Lehner et al., 2008) (left); Unit-catchments defined with a fixed-length river discretization, using a threshold of Δ𝑥 = 15 km) (right). Red points represent unit-catchment centroids where rainfall is interpolated.

S1.4 Channel geometry

For the assumption of a rectangular channel, river cross-section geometry is parameterized using downstream hydraulic geometry relationships (HG):

$$W_{bf_i} = aA_i^b$$
Eq. S1.4.1

$$D_{bf_i} = cA_i^d$$
Eq. S1.4.2

Where D_{bf_i} is the bankfull depth [m] for unit-catchment i; W_{bf_i} is the channel width [m] for unit-catchment i; A_i is the drainage area for unit-catchment i [km²]; a, b, c and d are fitting parameters, respectively, for river depth and width according to drainage area.

Table S1.4.1 and Figure S1.4.1 show an overview of channel geometries adopted for South America version of MGB, which were retrieved from literature. It is worth noting that Paiva et al., (2011, 2013) and Pontes (2016) are past applications of MGB model in Amazon

and La Plata basins, respectively.

Table S1.4.1. Sources of river geometry parameters (bankfull width and depth) for South American rivers.

Basin/River	Reference	River Geometry	Local adjustments
Amazon main stem (A_d> 2500000 km²)	Beighley and Gummaldi (2011)	HG based on drainage area	-
Japura, Negro, Solimoes, Xingu and Tapajos	Paiva et al., (2013)	HG based on drainage area	-
Purus and Jurua	Paiva et al., (2011)	HG based on drainage area	-
La Plata (Parana, Paraguay and Uruguay)	Pontes (2016)	*HG based on drainage area (Uruguay and Upper Parana basins) *Widths of main rivers obtained from Satellite imagery (Paraguay and lower Parana basins)	Bermejo River (A_d> 55000 km²): W = 270.82exp (–0.00005 A_d) Uruguay River (A_d > 50000 km²): W = 0.01$A_d^{0.95}$
Other South American Rivers	Andreadis et al., (2013)	HG based on mean annual peak flow	Sao Francisco river (A_d> 120000 km²): D = 12m

A_d = Drainage Area; W = Width; D = Depth;
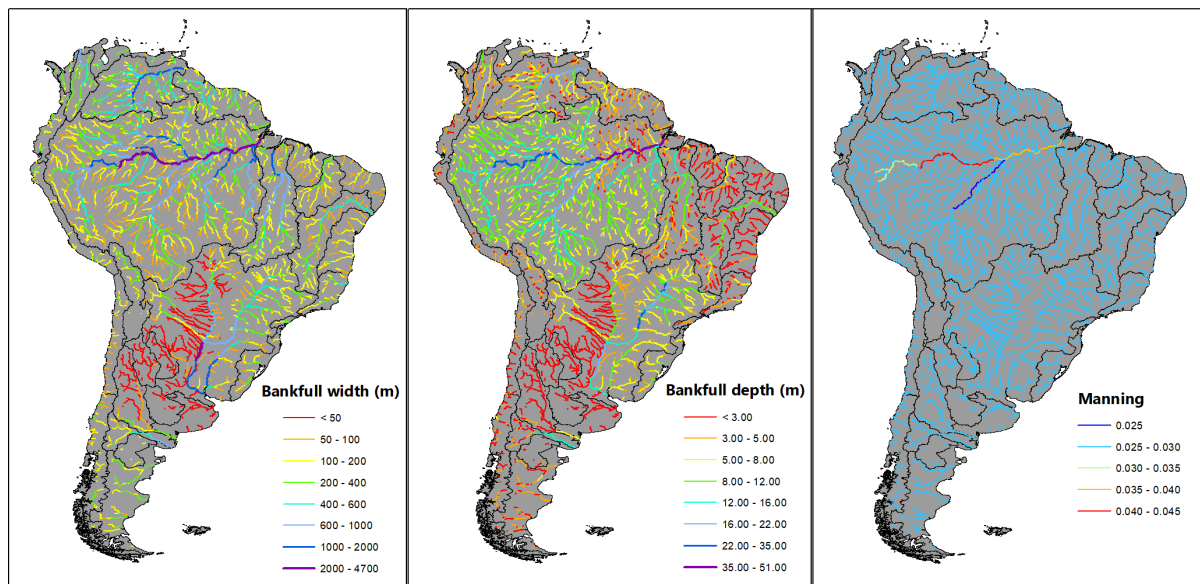
Figure S1.4.1. Adopted bankfull width and depth values based on works by Beighley e Gummaldi (2011), Andreadis et al., (2013), Paiva et al., (2011, 2013) and Pontes (2016). Manning coefficient was globally set to 0.03, with further adjustments based on Paiva et al., (2013)

A1.5 Adjustment of river bed profiles

River bed elevations (z in **Eq. S1.2.8**) are estimated subtracting the channel depths

from the river bank heights derived from a spaceborne DEM (in this case, the Bare-Earth SRTM version 1 DEM, (O'Loughlin et al., 2016)). However, for large-scale hydrodynamic routing it is essential to reduce noise in river bed profiles to avoid the excess of water leaving channels to the floodplains, especially when coarse resolution (both spatial and vertical) DEMs are used (Paiva et al., 2011; Yamazaki et al., 2012; Chen et al., 2018). Also, noise in river bed profiles are likely to be even more pronounced because of the superposition of HydroSHEDS drainage networks over the Bare-Earth SRTM, since the latter is not hydrologically corrected (for instance, after using a depression-filling correction (e.g. Jenson and Domingue, 1988)).

To handle this, we applied a noise reduction method based on a simple linear regression to obtain smoothed river bank heights. For a given unit-catchment, all DEM pixels located over the river reach of Δx = 15 km (according to fixed-length discretization) are used to adjust a linear regression. River bank height is set as the smoothed elevation associated to the center pixel of the river reach (**Figure S1.5.1**), without modifying DEM original values. Indeed, a larger benefit of the smoothing procedure is expected if a large number of pixels is sampled, i.e., by adopting a larger Δx, albeit this is not a good option due to the potential numerical instabilities associated to flow routing. **Figure S1.5.2** shows an example of the smoothed bed profile in comparison to the original one extracted from Bare-Earth SRTM (O'Loughlin et al., 2016).
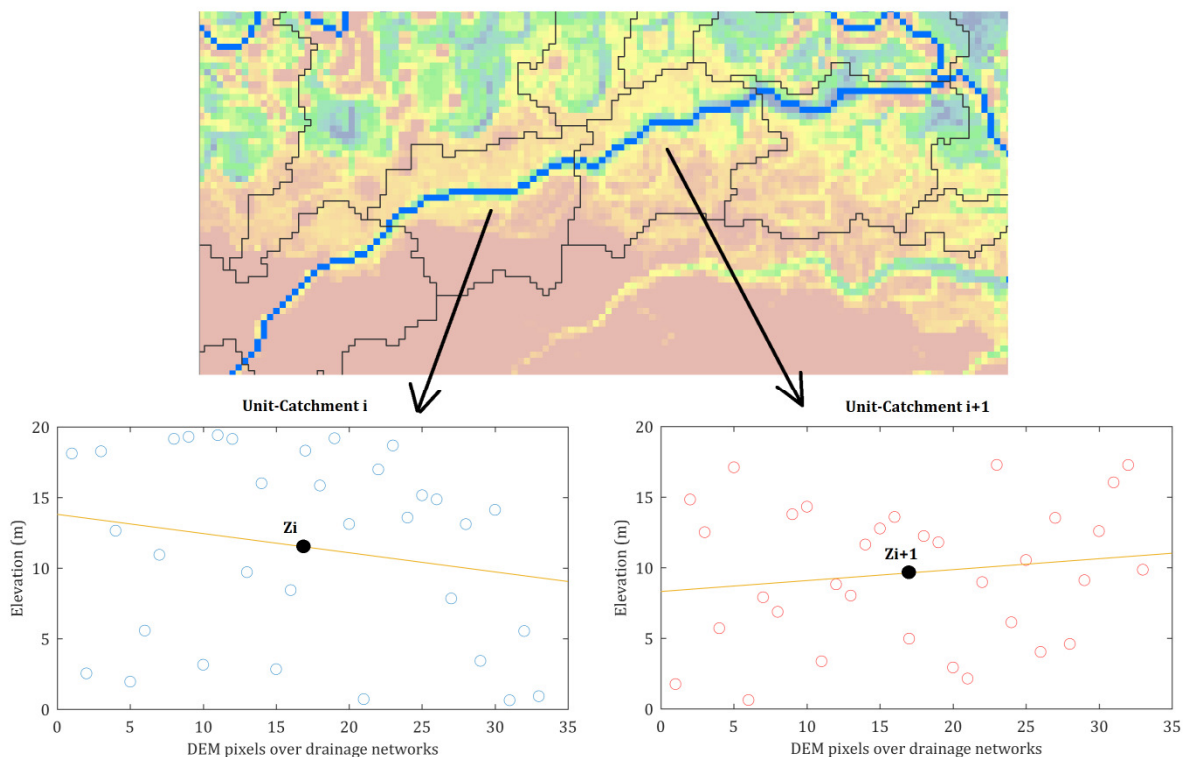
Figure S1.5.1. Schematic representation of noise reduction in river bed profiles. Circles represent the elevation of DEM pixels located over river networks, which are used to adjust a linear regression (yellow line) within a same unit-catchment. Pixel numbers are ordered from upstream to downstream, so that bank heights are set in the middle of river reaches using the linear regression slope.
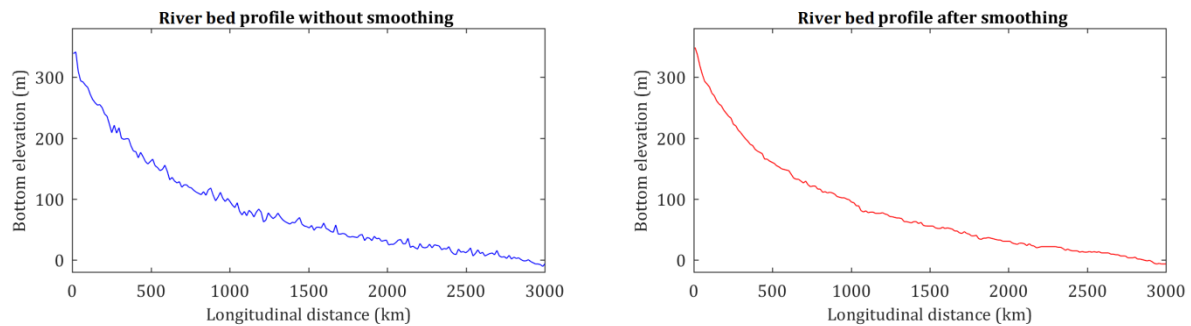
Figure S1.5.2. Comparison between non-smoothed (left) and smoothed (right) river bed profile extracted from Bare-Earth SRTM. River profiles in this example were extracted for Purus (380000 km²) mainstem, a tributary of the Amazon.

S1.6 Sub-grid (or sub- unit-catchment) floodplain topography

In order to represent floodplain inundation, a hypsometric curve relating flow depth, flooded area and water volume stored in both floodplain and channel for a given unit-catchment is derived from its underlying DEM. Regarding the floodplain, concepts of the HAND model (Rennó et al., 2008) were adopted to compute water volume emulating the inundation process from lower to higher elevations (**Figure S1.6.1**), which is the same approach adopted in CaMa-Flood by Yamazaki et al., (2013).

In this method, pixels characterized as main channels, i.e., over the drainage network, are initially set as null values defining the interface between channel bank height and floodplain region. The relative elevation between a given floodplain pixel and its nearest downstream channel pixel is computed as the height above channel top bank, which means that the pixel is only inundated if floodplain water level (current flow depth subtracted from channel bankfull depth) is equal or exceeds its respective HAND value. Thus, flooded area is calculated summing the individual areas of inundated pixels for a given HAND value, and volume of water stored in floodplain (plus channel below bankfull depth) is then computed considering vertical increments according to DEM vertical resolution. **Figure S1.6.2** shows a schematic representation of channel and floodplains (and their parameters) for a given unit-catchment.
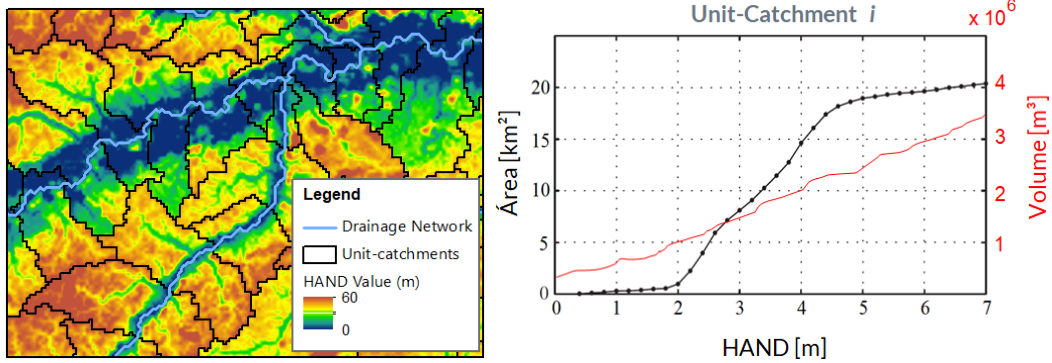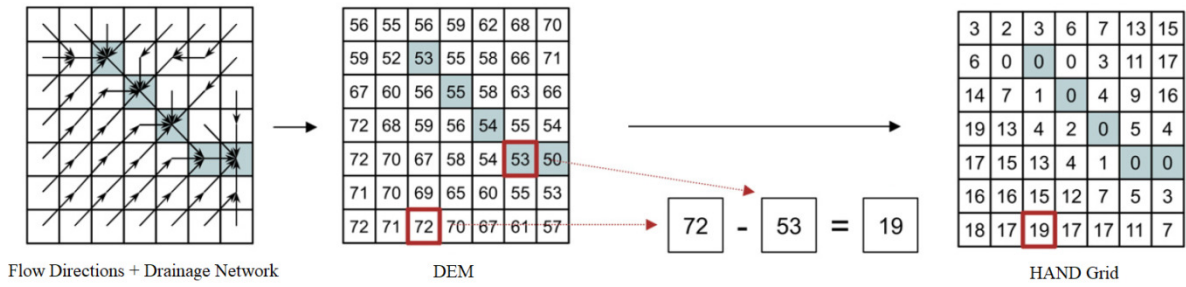
Figure S1.6.1. Procedure to compute sub-grid floodplain profile. Top: Derivation of HAND grid using flow directions, DEM and drainage map extracted from a given area threshold. White and shaded cells represent pixels located over floodplain and drainage networks (channel), respectively (adapted from Rennó et al., 2008). Bottom: Floodplain area and volume are obtained through vertical increments in the HAND Grid, within a given unit-catchment.
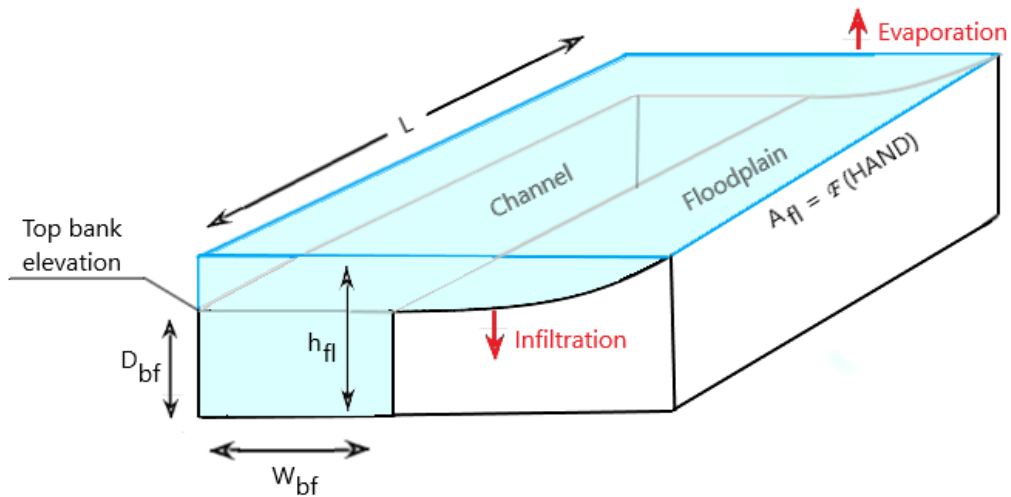
Figure S1.6.2. Schematic representation of channel and floodplain within a given unit-catchment. L = Channel length; D_{bf} = Bankfull depth; W_{bf} = Bankfull Width; h_{fl} = Flow depth; A_{fl} = Floodplain area, expressed as a function of HAND value (derived from sub-grid topography).

Following these assumptions, floodplain profiles relating HAND value to flooded area (A_{fl}) and flooded volume (V_{fl}) are defined as:

$$A_{fl}(z, i) = \sum_{\langle y,x\rangle \in S} A\langle y, x\rangle$$

Eq. S1.6.1

$$V_{fl}(z, i) = W_{bfi}D_{bfi}L_i + \sum_{k=1}^{z} 0.5\left[A_{fl}(k, i) + A_{fl}(k-1, i)\right]\Delta z$$

Eq. S1.6.2

Where z is the HAND value analyzed [m], i is the unit-catchment analyzed; A_{fl} is the flooded area above channel top bank, for a given HAND and unit-catchment [km²]; V_{fl} is the total water stored in the control volume (channel + floodplains), for a given HAND and unit-catchment [m³], $\langle y, x\rangle$ are the pixel coordinates, located at row y and column x, $A\langle y, x\rangle$ is the pixel surface area [m²], $S = \{\langle y, x\rangle | UC\langle y, x\rangle = i, HAND\langle y, x\rangle \leq z\}$, $UC\langle y, x\rangle$ is the pixel element from the unit-catchment grid; $HAND\langle y, x\rangle$ is the pixel element from the HAND grid [m], Δz is the vertical resolution of the HAND grid, equal to 1 m.

Finally, HAND values in the floodplain profile are further converted to water levels, in such a way that the latter are equivalent to HAND plus bankfull depth. For the submerged part of topography (i.e., inside channel), volume is calculated through the numerical integration of flooded area with flow depth, the former approximated by channel width times river length (Pontes et al., 2017). As described in **section S1.2**, this enables flow depths to be derived from stored water volume, by interpolating the channel/floodplain profile for a given unit-catchment.

S2. Structure of models (continental and global) evaluated in this study

General information about the structure of MGB continental model, as well as the global models HTESSEL/CaMa-Flood, LISFLOOD and WaterGAP3 is summarized in **Table S2.1**.

Table S2.1. Summary of the structure of models used in this study, acquired from eartH2Observe Water Resources Re-analysis run 2 (WRR-2) (Martinez-de la Torre et al., 2018).

Model	MGB	HTESSEL/CaMa-Flood	LISFLOOD	WaterGAP3
Interception	Single reservoir, potential evaporation	Single reservoir, potential evaporation	Single reservoir, potential evaporation	Single reservoir
Evaporation	Penman–Monteith	Penman–Monteith	Penman–Monteith	Priestley–Taylor
Snow	No	Energy balance, single layer (5 layers)	Degree-day, single layer	Degree-day, single layer
Soil layers	Single layer	9 layers	3 layers	Single layer
Groundwater	Yes	No	Yes	Yes
Runoff generation	Saturation excess	Saturation excess	Saturation and infiltration excess	Beta function
Reservoir/Lakes	No	No	Yes	Yes
Routing	1D inertial routing (Channel), floodplain as a storage	CaMa-Flood (1D inertial routing)	1D Double Kinematic wave (Channel + Floodplain)	Manning–Strickler
Vertical processes in floodplains	Evaporation and infiltration	No	No	No
Water use	No	No	Yes	Yes
Time step	1 day water and energy balance, CFL for routing	1 h	1 day	1 day
Grid/Sub-basin	Sub-basin (unit-catchments)	Grid	Grid	Grid
Model resolution	Fixed-length (15 km)	0.25º	0.1º	0.0833º (5 arc minutes)

S3. Metrics for individual continental and global models (considering all gauge stations)
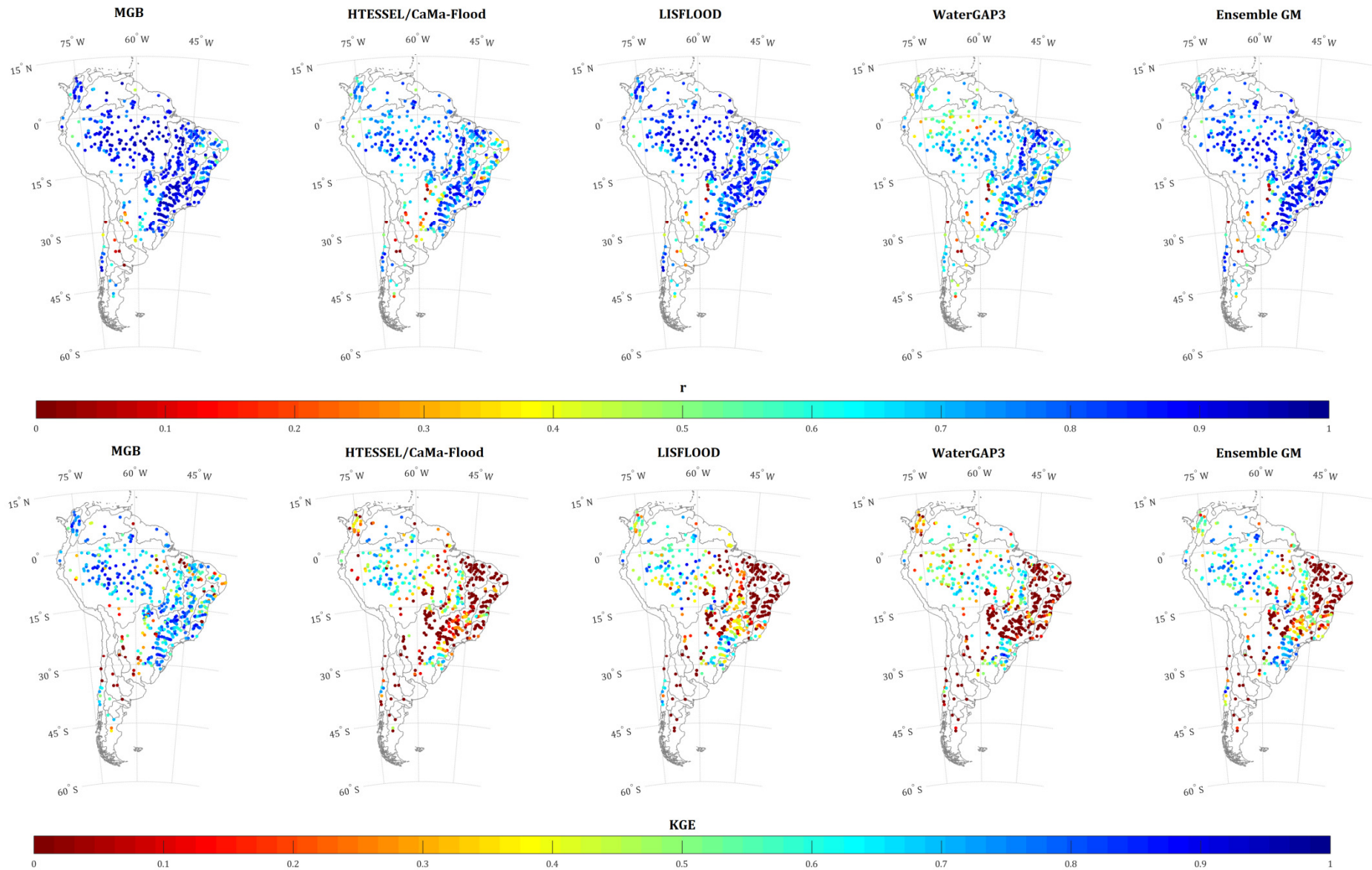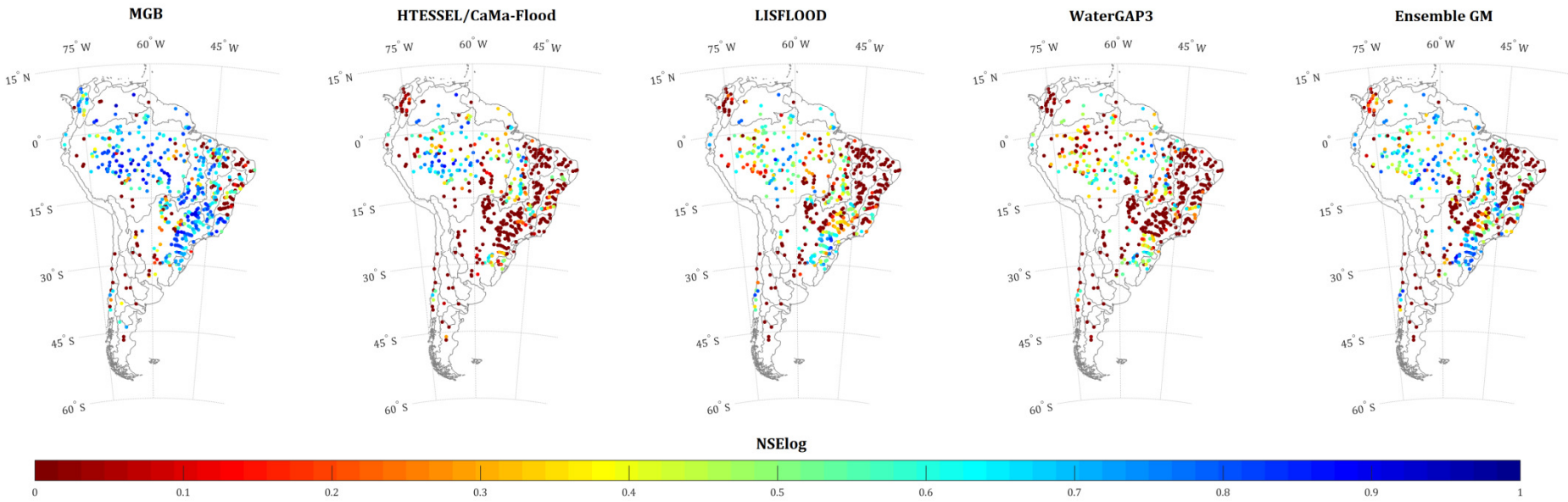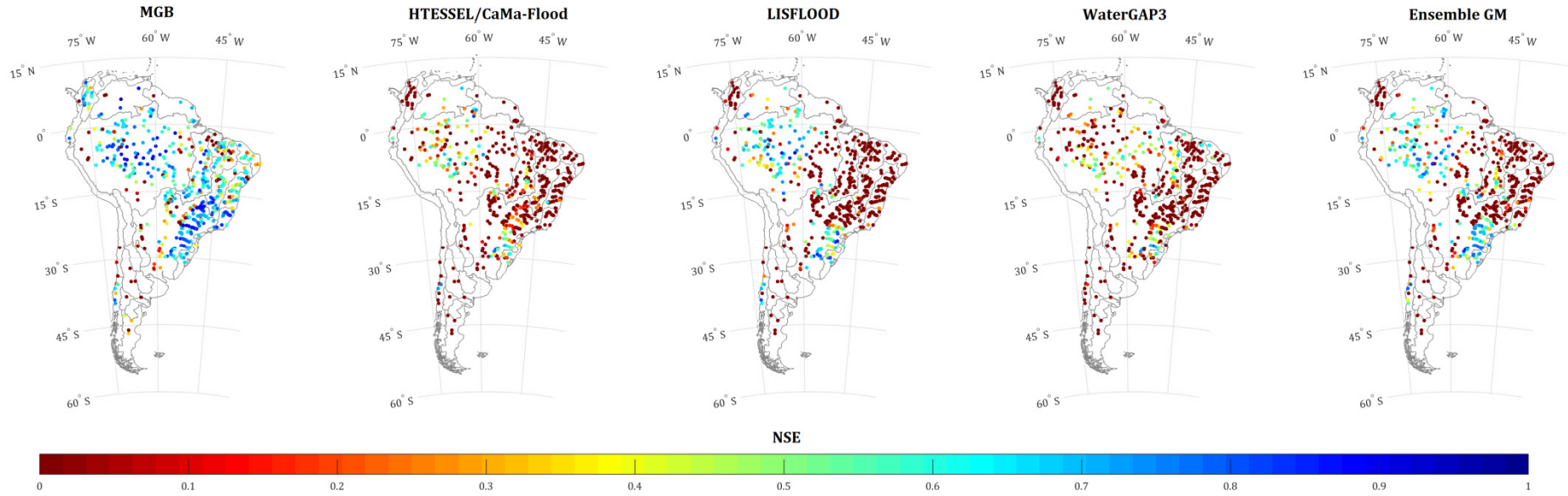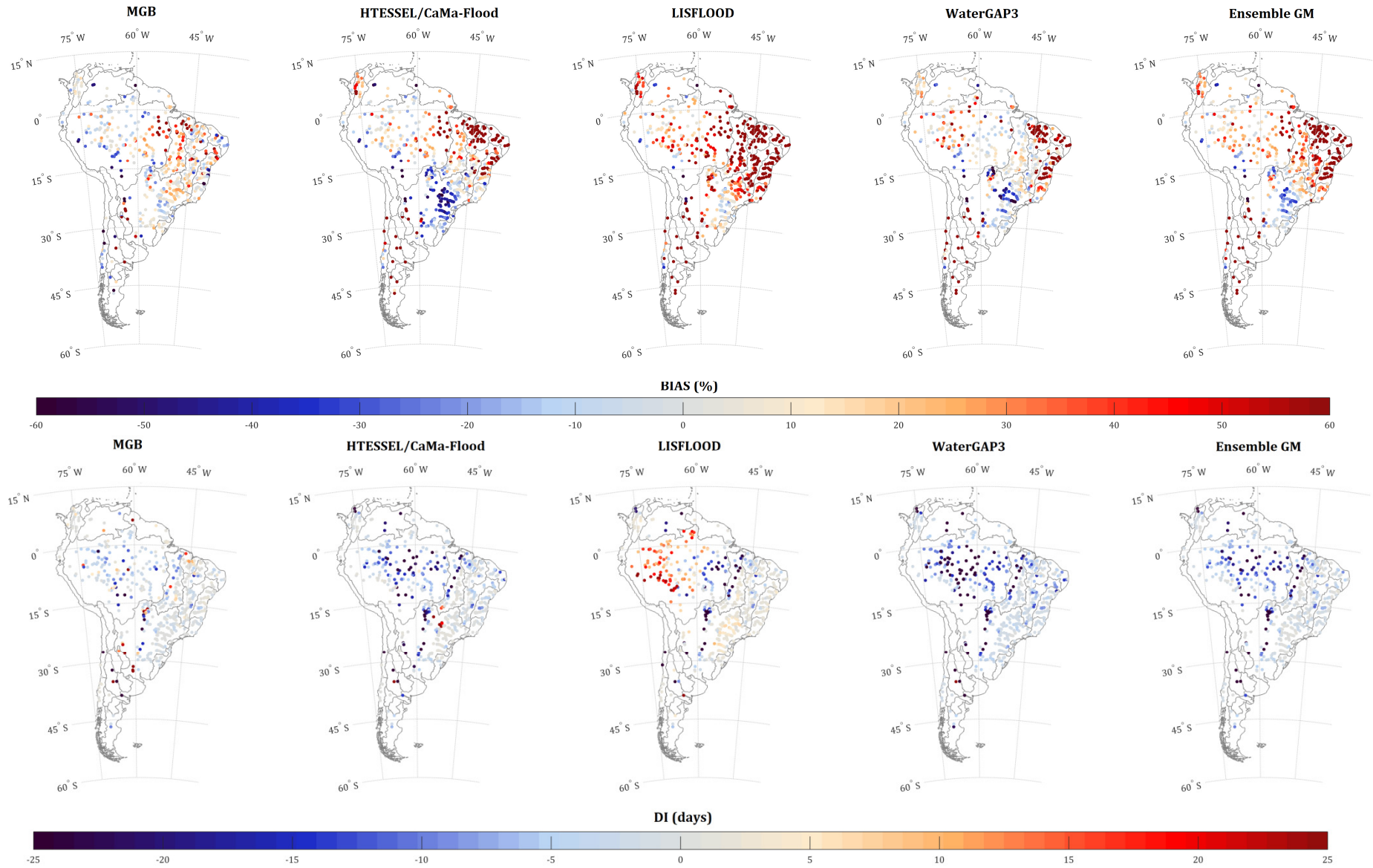
Additional References

Almeida, G. A. M., Bates, P., Freer, J. E., and Souvignet, M.: Improving the stability of a simple formulation of the shallow water equations for 2-D flood modeling, Water Resources Research, 48, 10.1029/2011WR011570, 2012.

Almeida, G. A. M., and Bates, P.: Applicability of the local inertial approximation of the shallow water equations to flood modeling, Water Resources Research, 49, 4833-4844, 10.1002/wrcr.20366, 2013.

Butt, M. A., and Maragos, P.: Optimum design of Chamfer distance transforms, IEEE Transactions on Image Processing, 7, 1477-1484, 10.1109/83.718487, 1998.

Beven, K.: Rainfall-Runoff Modelling: The Primer. Wiley, 448p, 2001

Chen, H., Liang, Q., Liu, Y., and Xie, S.: Hydraulic correction method (HCM) to enhance the efficiency of SRTM DEM in flood modeling, Journal of Hydrology, 559, 56-70, 10.1016/j.jhydrol.2018.01.056, 2018.

Cunge, J. A., Holly, F. M., and Verwey, A.: Practical aspects of computational river hydraulics. Pitman, 1980

Jenson, S. K., and Domingue, J. O.: Extracting topographic structure from digital elevation data for geographic information system analysis, Photogrammetric Engineering and Remote Sensing, 54, 1593-1600, 1988.

Maidment, D. R.: Arc Hydro: GIS for water resources. ESRI, 203p, 2002

Neal, J., Schumann, G., and Bates, P.: A subgrid channel model for simulating river hydraulics and floodplain inundation over large and data sparse areas, Water Resources Research, 48, 10.1029/2012WR012514, 2012.

Paz, A. R., and Collischonn, W.: River reach length and slope estimates for large-scale hydrological models based on a relatively high-resolution digital elevation model, Journal of Hydrology, 343, 127-139, 10.1016/j.jhydrol.2007.06.006, 2007.

Rawls, W. J., Ahuja, L. R., Brakensiek, D. and Shirmohammadi, A.: Infiltration and soil water movement, in: Handbook of Hydrology, edited by Maidment, D. R. McGraw-Hill, 1424p, 1993.

Shuttleworth, W. J.: Evaporation, in: Handbook of Hydrology, edited by: Maidment, D. R., McGraw-Hill, 1424p, 1993.

Wigmosta, M. S., Vail, L. W. and Lettenmaier, D. P.: A distributed hydrology-vegetation model for complex terrain. Water Resources Research, 30(6), 1665-1679, 1994.

Yamazaki, D., Baugh, C. A., Bates, P. D., Kanae, S., Alsdorf, D. E., and Oki, T.: Adjustment of a spaceborne DEM for use in floodplain hydrodynamic modeling, Journal of Hydrology, 436-437, 81-91, 10.1016/j.jhydrol.2012.02.045, 2012.